LANGMUIR

pubs.acs.org/Langmuir Article

Adsorption of P103 Nanoaggregates on Graphene Oxide Nanosheets: Role of Electrostatic Forces in Improving Nanosheet Dispersion

Rahul Patil, Debes Ray, Vinod K. Aswal, Cyrill Bussy, Pratap Bahadur, and Sanjay Tiwari*

Cite This: *Langmuir* 2021, 37, 867−873 Read Online

ACCESS | Metrics & More | Article Recommendations | Supporting Information

ABSTRACT: Graphene oxide (GO) nanosheet suspension is not stable in physiological ionic fluids. To improve stability, surfactants such as Pluronic 103 (P103) have been tested. Going further, this work investigated whether conferring positive surface charge to the surfactant may improve the adsorption ability of P103 micelles on GO sheets. Positive charge on the surfactant was induced by adding dodecyltrimethylammonium bromide (DTAB, a cationic surfactant) in P103 micelles. Subsequent changes in aggregation parameters were investigated through dynamic light scattering and small-angle neutron scattering studies. DTAB incorporation was accompanied by a steady increase in the ζ potential and mixed micelle formation. At high surface charge density, the interaction between adjacent head groups was distorted, which led to dissociation of mixed micelles. Structural developments during the adsorption of mixed micelles on the sheet surface (mass fractal formation) were monitored in terms of changes in the scattering features of aggregates. These fractals emerged as a result of electrostatic interactions. Our observations point toward the existence of small-sized building blocks at low DTAB concentration ($\leq$4 mM). With a superior adsorption, mixed micelles are expected to occupy the intersheet space and maintain a hydration layer. However, at a higher DTAB concentration ($\geq$10 mM), micelles dissociate to produce DTAB-rich unimers and P103-rich loose aggregates. At this point, sheets tend to aggregate in the solvent, regardless of fractal formation.

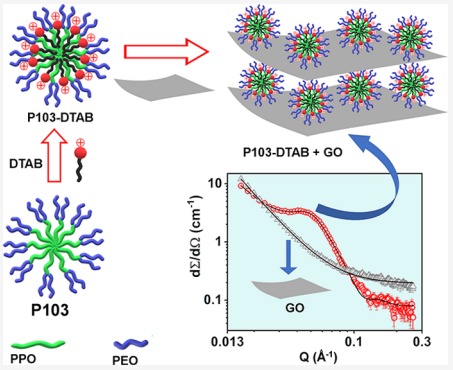

INTRODUCTION

Graphene oxide (GO) sheets possess negatively charged carboxyl groups, polar hydroxyl groups, and hydrophobic graphitic patches. Depending upon the specific method of synthesis, sheets exhibit heterogeneity in terms of layer number and interlayer structure.[1−3] Therefore, in spite of dense oxygen groups at the surface, high specific surface area and van der Waals (vdW) attractions result in the formation of irreversible aggregates in most physiological ionic solutions.[4]

The preventive approach largely relies on the use of amphiphilic block copolymers and surfactants for stabilizing the sheets via steric and electrostatic/electrosteric repulsions. As a result of noncovalent nature of these interactions, material properties of GO sheets remain unharmed.[2,5] In pre-micelle concentration regime, a hydrophobic segment of the block copolymer spreads over unoxidized regions of the GO sheet surface, whereas the hydrophilic counterpart dangles into the aqueous medium.[6] However, as the block copolymer concentration approaches the critical micelle concentration (CMC), the GO sheet surface is predominantly occupied by the micelles (mass fractal development). In a recent study, we showed that fractal aggregates of uncharged ethylene oxide−propylene oxide-based triblock copolymer Pluronic 103 (hereafter written as P103, CMC ∼ 0.37 wt %)[7] could sterically prevent the aggregation of GO sheets even after exposure to protein and electrolytes.[2] Other groups have instead used low-molecular weight surfactants during the GO exfoliation process. Given a shorter molecular length, low-molecular weight surfactants intercalate through the graphitic gallery and produce stable dispersions. Their nonpolar tail, polar head group, counterion, and aromatic substituents can be tuned to optimize the adsorption affinity. For instance, counterions in ionic surfactants can be substituted with aromatic ones in order to increase the hydrophobicity and reduce the CMC.[8]

Theoretical and experimental aspects of GO sheet−surfactant interactions have been studied by various research groups.[9−12] Atomistic simulations point toward random adsorption of surfactant molecules parallel to the sheet surface. However, as the surfactant concentration increases, the monolayer transforms to acquire a hemispherical shape.[12]

Received: November 4, 2020
Revised: December 24, 2020
Published: January 5, 2021

https://dx.doi.org/10.1021/acs.langmuir.0c03206
Langmuir 2021, 37, 867−873

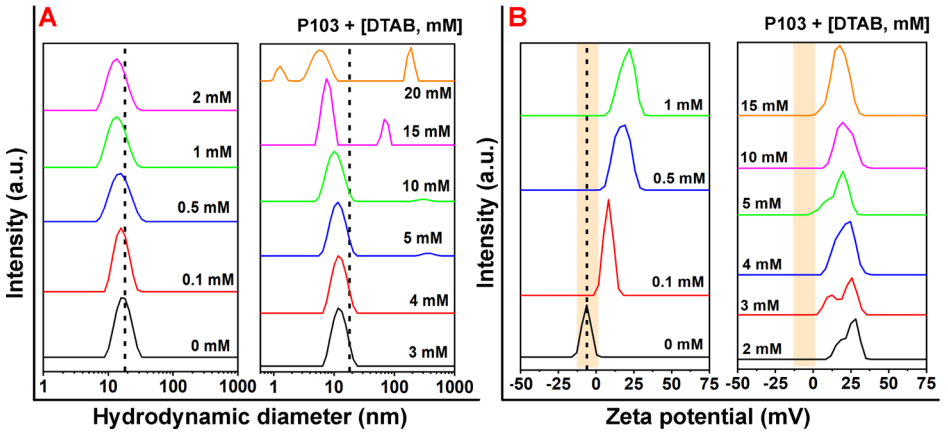

Figure 1. Changes in the hydrodynamic diameter (A) and ζ potential (ZP) (B) of P103 micelles upon DTAB addition. The data were acquired at room temperature.

Thermodynamic stability of such dispersions is dictated by the last confined layer of the surfactant molecule. This implies that GO sheets re-aggregate and tend to form thick multilayers because of desorption of the surfactant from the intersheet gap.[6] This poses a significant challenge for drug delivery applications of graphene oxide dispersion, including reduction in shelf life of the dispersion and agglomeration of GO sheets in physiological fluids.[2,13] Therefore, it is important to explore novel approaches for maintaining the dispersibility of GO sheets in aqueous media relevant to physiological application.

Looking at the density of carboxylic acid groups on GO sheets, we hypothesize that adsorption of micellar aggregates on the surface of GO would improve in the presence of cationic charge. This would be facilitated by the long operational range of electrostatic forces.[6] An analogy can be drawn from the strong influence of electrostatic forces during the interaction of GO with positively charged lipid membranes.[14] Similar observations have been recorded in positively charged inverse micelles loaded with GO sheets.[15] The micelles were composed of dodecyltrimethylammonium bromide (DTAB, CMC ∼ 15.4 mM), a cationic surfactant.[16] GO sheets migrated to the interface in the presence of DTAB. On the contrary, interfacial localization was not observed in the anionic surfactant assembly. Moreover, loss of negatively charged groups during reductive treatment of GO sheets lowers the stability by augmenting vdW forces.[17]

Encouraged by these findings, this study was planned to evaluate the effect of positive surface charge in mobilizing the P103 micelles to the GO surface. To test our hypothesis, cationic charge was introduced in P103 micelles via incremental addition of DTAB. Its effect was evaluated in terms of mass fractal development at the surface of GO sheets. The magnitude of positive charge was restricted to a low level (10−25 mV) in order to minimize the adsorption of oppositely charged species in the physiological environment.[18] Aggregates were characterized using dynamic light scattering (DLS) and small-angle neutron scattering (SANS).

MATERIALS AND METHODS

Materials. Graphite (>98% purity) was purchased from Loba Chemie, India. Sulfuric acid (98%), hydrochloric acid (35%), sodium nitrate (98% purity), potassium permanganate (99% purity), and hydrogen peroxide (30% w/v) were purchased from Rankem Laboratories, India. Solutions for SANS measurements were prepared in heavy water (99.9% purity) procured from Tokyo Chemical Industry, India. P103 (EO_{17}−PO_{60}−EO_{17}) was received as a gift sample from BASF Corp., USA. DTAB (>99% purity) was purchased from Sigma-Aldrich, USA. All other reagents were of analytical grade and used as received.

Methods and Characterizations. GO sheets were synthesized from graphite using a modified Hummers method, as described previously.[3,19] Mixed micelles (P103−DTAB) were prepared by adding different concentrations of DTAB (0.1−20 mM) to 1% solution of P103. Samples were analyzed for particle size distribution and zeta potential using Nano ZS, Malvern Instruments, UK. GO−micelle interactions were examined after adding a pre-weighed amount of GO (1 mg/mL) into micellar solutions.

SANS experiments were performed at Dhruva Reactor, Bhabha Atomic Research Centre, India. Measurements were performed after equilibrating the system at 30 °C (1 h). The mean wavelength of the monochromatized beam was 5.2 Å with a spread of $\Delta\lambda/\lambda \sim 15\%$. Angular distribution of scattered neutrons was recorded using a one-dimensional He3 position-sensitive detector. Data fitting and analyses were performed using the equations described in Supporting Information. Changes in dispersibility of GO were examined after adding DTAB into P103−GO dispersion.

RESULTS AND DISCUSSION

The study was divided into two parts: (a) development of positively charged P103−DTAB mixed micelles displaying unimodal size distribution and (b) investigation on the effect of positive charge upon adsorption of mixed micelles on the surface of GO sheet. Accordingly, we first investigated the effect of DTAB incorporation on micellar characteristics of nonionic P103. The apparent hydrodynamic diameter (D_h) of 1% P103 micelles at room temperature was recorded as 17 nm (polydispersity index < 0.2) (Figure 1A). It is clear from the size distribution plots that DTAB addition caused a progressive reduction in micelle size and favored micelle-to-unimer transition. At concentrations beyond 10 mM, DTAB-rich unimers and P103-rich loose aggregates were formed as a result of destabilization of mixed micelles.[20] The primary peak underwent broadening and/or splitting into two or three populations. The peak at ≈200 nm represents loosely bound aggregates of P103−DTAB mixed micelles, whereas unimers can be noticed at 2−3 nm.[21]

In order to ascertain the presence of unimers, we performed the DLS of neat DTAB (10 and 15 mM) solution. High-intensity unimers appeared at these concentrations without any evidence of self-assembled structures. Hence, it follows that aggregation of P103 was indeed altered by DTAB molecules. In a previous study, supramolecular structures were reported in

https://dx.doi.org/10.1021/acs.langmuir.0c03206
Langmuir 2021, 37, 867−873

F88 solution upon incorporation of cetyltrimethylammonium bromide, a cationic surfactant with four-carbon longer chain (C16) length. Authors argued that the hydrophobic chain avoided unfavorable contact with aqueous bulk by occupying the micelle core. Charged head groups were retained at the core−corona interface and imparted positive surface charge to the micelles.[22]

Micelle contraction at low DTAB concentration (<10 mM) can be attributed to hydrophobic engagement of DTAB with the PPO segment in the micelle core. Mixed micelles would have remained stable likely because of a balance between hydrophobic association and repulsive forces at the interface. However, at a higher DTAB concentration, surface charge density would have been increased. This can be understood by taking into account the fact that surface charge density of mixed systems depends on the aggregation number (N_{agg}) of ionic surfactants and size of the aggregates. Smaller aggregates composed of surfactants with higher N_{agg} possess higher charge density.[23] With its low critical packing parameter (<1/2), DTAB enhances the effective head group area in mixed micelles by virtue of its conical shape and charged head-groups.[24] Therefore, it may deregulate the interface to the point of dissociation.

The abovementioned argument of mixed micelle formation is well-supported by ZP measurements (Figure 1B). Devoid of ionizable groups, P103 micelles exhibited near-zero ZP (−3 mV). It steadily shifted to an overall positive charge as the concentration of DTAB was increased. This indicates the alteration in local Coulomb forces and emergence of surface charge on the micelle surface.[25] An opposite trend is typically observed during neutralization of surface charge.[26] In the Smoluchowski limit, ZP of the aggregate scales linearly with the surface charge density and is indirectly proportional to the area occupied by the charged functional group.[27] Given that the latter remains constant in our case, increase in ZP is indicative of changes in charge density. At a higher concentration, DTAB caused substantial peak broadening and subsequent splitting in the distribution plot. For example, two distinct peaks (+10.7 and +21 mV) can be seen with 3 mM DTAB. However, zeta potential became constant beyond 3 mM DTAB. Altogether, DLS studies clarify that addition of positive charge in P103 micelles can be achieved through inclusion of DTAB.

SANS data shed more light on structural features of P103 micelles upon DTAB incorporation. The experimental data were fitted to the spherical core−shell model. In order to better describe the influence of DTAB, we have classified the results in low (<4 mM), moderate (4−10 mM), and high (≥10 mM) concentration regimes. To begin with, the spherical shape of the neat P103 micelle can be confirmed from the bell shape of its pair-distance distribution function, $p(r)$ (Figure S1). P103−DTAB data show no noticeable change in the scattering profile of micelles in the low DTAB regime (Figure 2A). At the moderate concentration, DTAB caused reduction in scattering intensity and shift of the correlation peak to a higher Q region (Figure 2B). Looking at the calculated structural parameters (Table 1), we suggest that reduction in scattering intensity originated from the contraction of the micelle core along with lowering in the aggregation number (N_{agg}) of P103. As a result, the number density of micelles increased up to fivefold. The numerical value of scattering length density highlights the contrast existing among core,

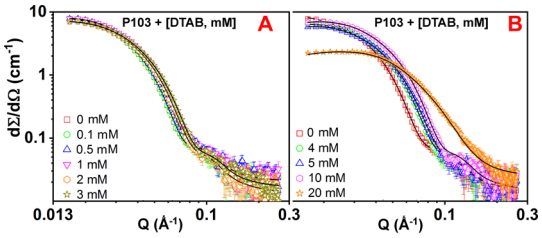

Figure 2. Changes in the neutron scattering profile of P013 micelles upon DTAB addition. Shown are the data for DTAB concentration ranging from 0.1−3 mM (A) and 3−20 mM (B). The scattering data were fitted to the sphere core−shell model.

shell, and dispersion medium (heavy water) during data acquisition.[28]

In nonionic assemblies, contraction of the core and lowering in N_{agg} at a fixed amphiphile concentration have been linked to increase in number density.[29] Therefore, we believe that peak shift in the high Q region might have occurred because of appearance of additional micelles and reduction in the intermicellar distance. In spite of this, micelles did not associate to form large aggregates, most likely as a result of surface charge imparted by DTAB molecules. As stated before, charge density of aggregates would depend on N_{agg} of DTAB and the size of the mixed micelles. This implies that higher N_{agg} of DTAB would be conducive to higher effective charge (e) and greater separation among the micelles.[30] Changes in the aggregation pattern at 15 and 20 mM DTAB can be attributed to saturation in the solubilization ability of P103 micelles that led to excessive charge build-up in the shell region.[25] As a result, micelles were destabilized to form DTAB-rich unimers and P103-rich loose clusters (Figure 1A).

Next, we obtained the interparticle structure factor [$S(Q) = 2\pi/d$] by dividing the scattering contribution of mixed aggregates with that of bare P103 micelles. It displays a pronounced correlation peak and has been used to delineate the micelle−micelle interaction.[30,31] We modeled the $S(Q)$ factor of interacting micelles using the Hayter−Penfold system.[30] As against to absence of $S(Q)$ until 2 mM, its appearance can clearly be noticed after 3 to 10 mM DTAB. A modest increase in the peak height can be noticed between 3 to 10 mM (Figure 3). It corroborates our hypothesis that because of the formation of small-sized micelles (high number density), the intermicellar distance decreased. The data shown in Table 1 suggest that aggregation of micelles would have been prevented by the appearance of effective charge.

With these observations, it becomes clear that optimum positive charge can be achieved in P103 micelles with the use of 3 mM DTAB without triggering unimerization or loose cluster development. We then proceeded with the investigation on adsorption ability of positively charged P103−DTAB micelles on the surface of GO sheets. A comparison between the neutron scattering profile of GO sheets in pure P103 and that in pure DTAB is shown in Figure 4. Whereas P103 micelles were fitted to the spherical core−shell model, scattering data of GO powder showed a good fit to the mass fractal model. In agreement with our earlier work,[32] scattering data of P103−GO were fitted to a combination of the spherical core−shell and mass fractal models. Apart from shift in the scattering peak to the high Q region, sheet incorporation was accompanied with hump formation (Figure 4A). Other noteworthy observations include reduction of the aggregation number (41 from 166), shrinkage of micelles (3.8 from 6.1

https://dx.doi.org/10.1021/acs.langmuir.0c03206
Langmuir 2021, 37, 867−873

Table 1. SANS-Derived Structural Parameters of P103 Micelles at the Increasing Concentration of DTAB[a]

DTAB (mM)	R_c (nm)	R_{hs} (nm)	α (esu)	Φ	PD	N_{agg}		N × 10^{16} (cm^{-1})	SLD (×10^{10} cm^{-2})	
						P103	DTAB		core	shell
0.0	6.1				0.16	166	0	0.389	0.32	0.63
0.1	6.1				0.17	165	8		0.32	0.63
0.5	5.9		22.34		0.17	148	37		0.31	0.62
1.0	5.7		26.04		0.17	133	66		0.31	0.60
2.0	5.5		24.18		0.17	124	123		0.30	0.58
3.0	5.3		15.47		0.18	109	162		0.29	0.55
4.0	5.2		21.13		0.17	101	201		0.28	0.53
5.0	4.9	7.4	24.61	0.03	0.19	87	215	1.65	0.27	0.51
10.0	4.7	8.5	20.98	0.05	0.18	77	380	2.00	0.24	0.42
20.0	2.9	5.4	12.19	0.06	0.35	18	174	8.87	0.20	0.32

[a] R_c—core radius, R_{hs}—hard sphere radius, α—effective charge, Φ—volume fraction, PD—polydispersity, N_{agg}—aggregation number, N—number density of micelles, SLD—scattering length density.

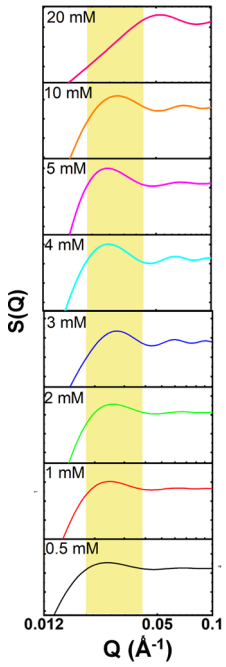

Figure 3. Changes in $S(Q)$ of P103 micelles upon DTAB addition. The numerical value on Y-axis was kept identical in order to present the changes clearly.

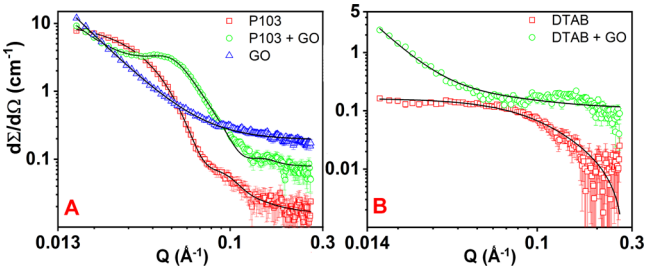

Figure 4. Neutron scattering profile of P103 micelles upon GO addition. The data of P103 micelles were fitted to the spherical core−shell model. GO powder fitted best to the mass fractal model. P103−GO dispersion was fitted with a combination of core−shell sphere and mass fractal models (A). Scattering profiles of DTAB (20 mM) and DTAB−GO are shown in (B). Whereas the data of DTAB dispersion were fitted to the ellipsoid core−shell model, the data of DTAB−GO dispersion were fitted to a combination of ellipsoid core−shell and mass fractal models.

nm), and more than 60-fold increase in the number density of micelles (Table S1). We speculate that additional small-sized micelles would cover the sheet surface and form the fractal structure. The hump in the scattering profile of P103−GO dispersion can be ascribed to the structure factor that emerged as a result of the micelle−sheet interaction. In such an interaction, micelles are either adsorbed on the surface or trapped between the GO sheets.[5,32]

We observed ellipsoidal core−shell micelles in the case of pure DTAB (20 mM) solution (Figure 4B). Semi-major and semi-minor axis of micelles were found to be 2.17 and 1.9 nm, respectively. These micelles were adsorbed on the GO surface and produced fractal structures with 2.85 fractal dimension (Table S2). The latter is verifiable from the fit of scattering data to ellipsoidal core−shell and mass fractal combination. Apparently, the adsorption was driven through electrostatic attraction between the negatively charged sheet surface and the cationic DTAB head group.[9,15] In spite of this, the dispersion showed poor stability, suggesting that fractal development cannot be an absolute indicator of higher dispersibility. It, thus, poses a question on the ability of surfactant structures in effectively masking the effect of hydrophobic patches present at the surface of GO sheet.[3] This has been illustrated in the study by McCoy et al.,[5] who argued that cationic unimers adsorb via head groups which push the hydrophobic tail into bulk aqueous medium. Entropic factors allow for the alignment of another surfactant molecule in antiparallel orientation ("head-out" direction), wherein energetically favorable tail−tail association occurs. However, as the local crowding occurs, unimer adsorption is hindered because of two factors: (a) compensation of surface charge among vertically arranged surfactant units and (b) shielding of the surface in the event of lateral stretching of the surfactant tail.[33] In such a situation, desirable aqueous dispersibility may not be achieved in spite of surfactant adsorption. In our case, it was evident from precipitation of GO sheets within 4 h when 10 mM DTAB was used (data not shown).

The data of GO sheet dispersion in mixed micelles were fitted using the combination of mass fractal and spherical core−shell models. Features related to the overall size of aggregates (lower Q cut-off) could not be observed within the Q range of the present measurements. Instead, we have considered a fixed overall size (greater than $2\pi/Q_{min}$) for the analysis.[34] In the case of inorganic nanoparticles (size < 100 nm), improvement in the dispersibility has been investigated in terms of changes in fractal dimension, type of the building

https://dx.doi.org/10.1021/acs.langmuir.0c03206
Langmuir 2021, 37, 867−873

block, radius of aggregates, and overall size of fractal aggregates.[35,36] Calculation of these different parameters could not be performed in our case because of co-existence of multiple structures (mixed micelles, unimers, loose aggregates, etc.). Therefore, we have used a summation model (Figures S2−S4) for data fitting. The fitting procedure involved a mass fractal model for the low Q region and a sphere core−shell model (with the Hayter Penfold structure factor) for mid- and high Q region data.[5]

A comparison between the scattering profiles of P103 and mixed micelles clearly highlights the role of positive change upon aggregate adsorption (Figure 5A,B). In order to understand the changes comprehensively, we split the scattering profile into low (0.016−0.037 Å), middle (0.038−0.059 Å), and high (0.060−0.1 Å) Q regions. Scattering at low- and high Q, respectively, is controlled by the fractal aggregates and micelles. On the other hand, the middle Q region is contributed by the building block representing P103−DTAB/GO aggregates.[36] Existence of fractal structures in the low Q region can be confirmed from a linear scattering profile.[37] As stated earlier, these fractals would have developed either through micelle adsorption on the sheet surface (hump-like build-up in middle Q) or following their confinement between the sheets (higher scattering in low Q).[34]

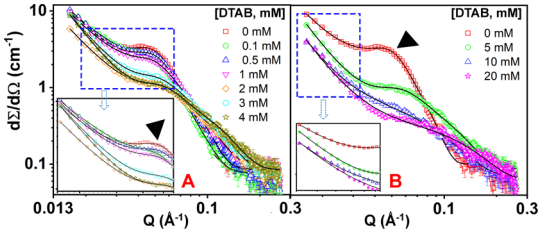

Figure 5. Changes in the neutron scattering profile of P103−GO dispersion with varying concentrations of DTAB. It shows the scattering profile of aggregates containing charged mixed micelles (A). The effect of micelle dissociation can be noticed in (B). The data were fitted with spherical core−shell and mass fractal models.

Increase in the width of scattering build-up during DTAB addition indicates enhancement in the attractive interaction between GO sheets and mixed micelles. Intriguingly, as the DTAB concentration increased, the hump underwent reduction (5 mM) and complete disappearance (≥10 mM; Figure 5A,B). This is indicative of disruption in the aggregate−sheet interaction beyond a threshold DTAB concentration (4 mM). In addition, the data highlight premature disruption of micelles in the presence of GO sheets. This was confirmed by subtracting the contribution of mass fractal scattering from the fitted data (P103−DTAB + GO). Here, the fitted line represents the sphere model along with Hayter−Penfold structure factor (Figure S5). It appears that, responding to GO sheet hydrophobicity, mixed micelles were depleted from the bulk solution and they covered the hydrophobic points.[5] The involvement of the electrostatic interaction between the sheet and mixed micelles can be verified from the drop in ZP (up to 8−12 mV) of the dispersion (Figure S6).

Considering the changes in size of P103 micelles during DTAB incorporation and the affinity of mixed micelles for the GO sheet surface, changes in the size of fractal aggregates can be expected.[38,39] Accordingly, we are proposing a plausible mechanism for the formation of small-sized compact building blocks (Figure 6).

We assume that micelle adsorption would minimize the intersheet interaction and increase the interlayer distance (Figure 6A). Given a highly hydrated corona, it is expected that a sub-nanometer thick hydration layer would be maintained at the surface of GO sheets.[40] The minimum intersheet distance in such surface-separated structures would be equivalent to the micelle diameter (8.5 to 12 nm). This is analogous to a mechanism of GO sheet stabilization demonstrated by Lambert's group[41] who employed pyrene−

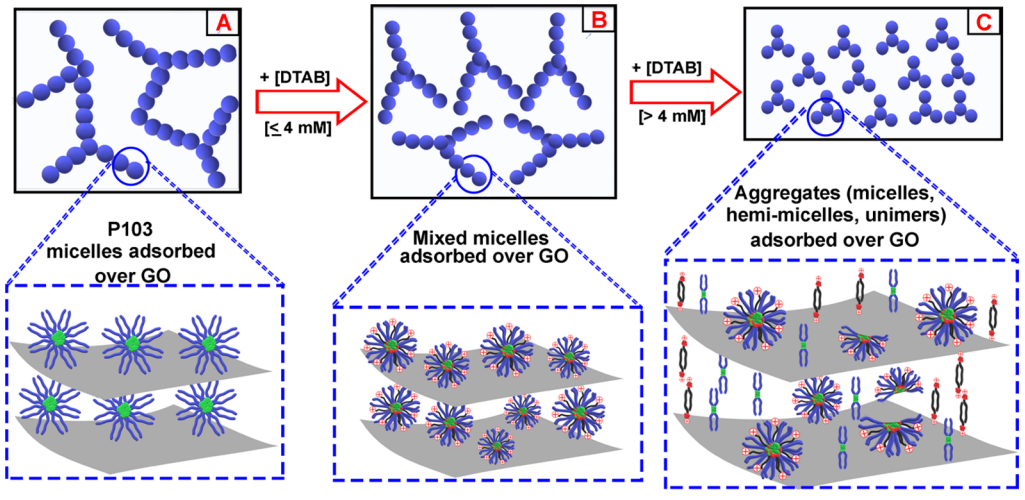

Figure 6. Scheme showing the mechanism of sheet stabilization through adsorption of neutral and positively charged aggregates. Initially, P103 micelles occupied the surface and formed fractal aggregates (A). Later, the fractal dimension and building block radius varied in accordance with the DTAB concentration. At low concentration (≤4 mM), the surface was covered by positively charged mixed micelles in high number density. In comparison to (A), the building block radius of aggregates (per fractal structure) would be lower. Eventually, the overall size of fractal aggregates would reduce, thereby leading to emergence of densely packed structures in the medium. At this point, aqueous dispersity would be higher because of high affinity between negatively charged sheets and positively charged aggregates (B). However, as the DTAB concentration became high (≥4 mM), the sheet surface would be occupied by unimers and loose assemblies derived from the dissociated mixed micelles (C). The steric barrier would break, thereby triggering the aggregation of sheets.

https://dx.doi.org/10.1021/acs.langmuir.0c03206
Langmuir 2021, 37, 867−873

oligoethylene glycol-based surfactants. Atomically flat sheets were initially occupied by planar starfish micelles. At a higher concentration, surfactant molecules clustered to form discrete conical structures which eventually acted as an intersheet barrier.

In the present study, an important finding is related to a reduction in the building block (GO sheets covered by mixed micelles) radius at a moderate DTAB concentration (≤4 mM). We hypothesize that until this concentration, DTAB would reduce the number of building blocks per fractal structure. This is accompanied by an increase in the number density of small-sized fractal structures (in sync with the increased number density of micelles, Table 1). Reduction in fractal size is verifiable from the scattering build-up[36] at the low Q region shown in Figure 5. Eventually, the number density of fractals contributes to higher fractal dimension. However, at high concentration (>10 mM, for instance), DTAB probably destabilized the aggregates into unimers, clusters, or other aggregates which exhibited low affinity for the GO sheets (Figure 6B,C). We qualitatively verified that superior aqueous dispersibility of GO sheets was attained with mixed micelles containing <4 mM DTAB.

CONCLUSIONS

In the present work, adsorption affinity of positively charged mixed micelles (P103−DTAB) on anionic GO sheets has been investigated as a function of DTAB addition. Incorporation of DTAB correlated with the appearance of positive charges at the surface of P103 micelles until the point of destabilization. Our observations reveal that charged micelles occupied the sheet surface via the electrostatic interaction and produced fractal structures. The effect of DTAB addition was clearly visible in fractal structures. At low concentration (≤4 mM), DTAB stimulated formation of smaller micelles in the high number density, which were effectively adsorbed on the GO sheets to produce dense building blocks. These P103−DTAB aggregates acted as an intersheet barrier while engaging with the dispersion medium. Such an arrangement is expected to minimize the intersheet interactions. However, the building blocks became loose, as the concentration of DTAB was increased beyond 4 mM. In future works, it will be interesting to study the stability of this achieved P103−DTAB−GO dispersion in physiological fluids.

ASSOCIATED CONTENT

Supporting Information

The Supporting Information is available free of charge at https://pubs.acs.org/doi/10.1021/acs.langmuir.0c03206.

SANS analysis; calculation of the aggregation number and number density of mixed micelles; fitting procedure of the summation model; subtraction of mass fractal contribution from the scattering data; ZP of mixed micelles upon adsorption on GO sheets; scattering parameters of P103 micelles in association with GO sheets; and scattering parameters of DTAB unimers in association with GO sheets (PDF)

AUTHOR INFORMATION

Corresponding Author

Sanjay Tiwari − *Maliba Pharmacy College, UKA Tarsadia University, Surat 394350, India;* orcid.org/0000-0001-7898-7974; Phone: 91-2625-255882; Email: tiwarisanju@gmail.com; Fax: 91-2625-255882

Authors

Rahul Patil − *Maliba Pharmacy College, UKA Tarsadia University, Surat 394350, India*

Debes Ray − *Solid State Physics Division, Bhabha Atomic Research Centre, Mumbai 400085, India;* orcid.org/0000-0001-5564-2973

Vinod K. Aswal − *Solid State Physics Division, Bhabha Atomic Research Centre, Mumbai 400085, India;* orcid.org/0000-0002-2020-9026

Cyrill Bussy − *Nanomedicine Lab, School of Biological Sciences, and Lydia Becker Institute of Immunology and Inflammation, Faculty of Biology, Medicine & Health, The University of Manchester, Manchester Academic Health Science Centre, Manchester M13 9PR, U.K.; National Graphene Institute, The University of Manchester, Manchester M13 9PR, U.K.;* orcid.org/0000-0001-8870-443X

Pratap Bahadur − *Department of Chemistry, Veer Narmad South Gujarat University, Surat 395007, India*

Complete contact information is available at: https://pubs.acs.org/10.1021/acs.langmuir.0c03206

Author Contributions

R.P.: investigation and writing—original draft. D.R.: formal analysis. V.K.A.: formal analysis. C.B.: writing—review and editing. P.B.: writing—review and editing. S.T.: conceptualization, writing—review and editing, and project administration.

Notes

The authors declare no competing financial interest.

ACKNOWLEDGMENTS

S.T. thanks the Science & Engineering Research Board (SERB), New Delhi, for funding under the ECRA scheme (# ECR/2017/000903). DLS facility at Maliba Pharmacy College is funded by DST-FIST, New Delhi.

REFERENCES

(1) Lin, S.; Shih, C.-J.; Strano, M. S.; Blankschtein, D. Molecular insights into the surface morphology, layering structure, and aggregation kinetics of surfactant-stabilized graphene dispersions. *J. Am. Chem. Soc.* **2011**, *133*, 12810−12823.

(2) Patil, R.; Bahadur, P.; Tiwari, S. Dispersed graphene materials of biomedical interest and their toxicological consequences. *Adv. Colloid Interface Sci.* **2020**, *275*, 102051.

(3) Patil, R.; Patel, H.; Pillai, S. B.; Jha, P. K.; Bahadur, P.; Tiwari, S. Influence of surface oxygen clusters upon molecular stacking of paclitaxel over graphene oxide sheets. *Mater. Sci. Eng., C* **2020**, *116*, 111232.

(4) Nazari, B.; Ranjbar, Z.; Hashjin, R. R.; Rezvani Moghaddam, A.; Momen, G.; Ranjbar, B. Dispersing graphene in aqueous media: Investigating the effect of different surfactants. *Colloids Surf., A* **2019**, *582*, 123870.

(5) McCoy, T. M.; De Campo, L.; Sokolova, A. V.; Grillo, I.; Izgorodina, E. I.; Tabor, R. F. Bulk properties of aqueous graphene oxide and reduced graphene oxide with surfactants and polymers: adsorption and stability. *Phys. Chem. Chem. Phys.* **2018**, *20*, 16801−16816.

(6) Hong, B. J.; Compton, O. C.; An, Z.; Eryazici, I.; Nguyen, S. T. Successful stabilization of graphene oxide in electrolyte solutions: enhancement of biofunctionalization and cellular uptake. *ACS Nano* **2012**, *6*, 63−73.

(7) Fernandez, V. V. A.; Soltero, J. F. A.; Puig, J. E.; Rharbi, Y. Temporal evolution of the size distribution during exchange kinetics of pluronic P103 at low temperatures. *J. Phys. Chem. B* **2009**, *113*, 3015−3023.
(8) Mohamed, A.; Ardyani, T.; Abu Bakar, S.; Sagisaka, M.; Umetsu, Y.; Hamon, J. J.; Rahim, B. A.; Esa, S. R.; Abdul Khalil, H. P. S.; Mamat, M. H.; King, S.; Eastoe, J. Rational design of aromatic surfactants for graphene/natural rubber latex nanocomposites with enhanced electrical conductivity. *J. Colloid Interface Sci.* **2018**, *516*, 34−47.
(9) Meng, W.; Gall, E.; Ke, F.; Zeng, Z.; Kopchick, B.; Timsina, R.; Qiu, X. Structure and interaction of graphene oxide−cetyltrimethylammonium bromide complexation. *J. Phys. Chem. C* **2015**, *119*, 21135−21140.
(10) Cao, J.; Bai, X.; Ye, Z.; Chen, W.; Ge, H.; Ding, Y.; Hua, Z. Enhanced transport of TiO2-reduced graphene oxide nanocomposites in saturated porous media: the impact of loaded TiO2 shape and solution conditions. *Water, Air, Soil Pollut.* **2020**, *231*, 124.
(11) Ardyani, T.; Mohamed, A.; Bakar, S. A.; Sagisaka, M.; Umetsu, Y.; Mamat, M. H.; Ahmad, M. K.; Khalil, H. P. S. A.; King, S.; Rogers, S. E.; Eastoe, J. Surfactants with aromatic headgroups for optimizing properties of graphene/natural rubber latex composites (NRL): Surfactants with aromatic amine polar heads. *J. Colloid Interface Sci.* **2019**, *545*, 184−194.
(12) Poorsargol, M.; Alimohammadian, M.; Sohrabi, B.; Dehestani, M. Dispersion of graphene using surfactant mixtures: Experimental and molecular dynamics simulation studies. *Appl. Surf. Sci.* **2019**, *464*, 440−450.
(13) Huang, C.; Wu, J.; Jiang, W.; Liu, R.; Li, Z.; Luan, Y. Amphiphilic prodrug-decorated graphene oxide as a multi-functional drug delivery system for efficient cancer therapy. *Mater. Sci. Eng., C* **2018**, *89*, 15−24.
(14) Frost, R.; Jönsson, G. E.; Chakarov, D.; Svedhem, S.; Kasemo, B. Graphene oxide and lipid membranes: interactions and nanocomposite structures. *Nano Lett.* **2012**, *12*, 3356−3362.
(15) Das, K.; Maiti, S.; Ghosh, M.; Mandal, D.; Das, P. K. Graphene oxide in cetyltrimethylammonium bromide (CTAB) reverse micelle: a befitting soft nanocomposite for improving efficiency of surface-active enzymes. *J. Colloid Interface Sci.* **2013**, *395*, 111−118.
(16) Bergström, L. M.; Aratono, M. Synergistic effects in mixtures of two identically charged ionic surfactants with different critical micelle concentrations. *Soft Matter* **2011**, *7*, 8870−8879.
(17) Gudarzi, M. M. Colloidal stability of graphene oxide: aggregation in two dimensions. *Langmuir* **2016**, *32*, 5058−5068.
(18) Sharma, R.; Baik, J. H.; Perera, C. J.; Strano, M. S. Anomalously large reactivity of single graphene layers and edges toward electron transfer chemistries. *Nano Lett.* **2010**, *10*, 398−405.
(19) Patil, R.; Kansara, V.; Ray, D.; Aswal, V. K.; Jha, P. K.; Bahadur, P.; Tiwari, S. Slow degrading hyaluronic acid hydrogel reinforced with cationized graphene nanosheets. *Int. J. Biol. Macromol.* **2019**, *141*, 232−239.
(20) Thummar, A. D.; Sastry, N. V.; Verma, G.; Hassan, P. A. Aqueous block copolymer−surfactant mixtures—Surface tension, DLS and viscosity measurements and their utility in solubilization of hydrophobic drug and its controlled release. *Colloids Surf., A* **2011**, *386*, 54−64.
(21) Parmar, A.; Chavda, S.; Bahadur, P. Pluronic−cationic surfactant mixed micelles: Solubilization and release of the drug hydrochlorothiazide. *Colloids Surf., A* **2014**, *441*, 389−397.
(22) Singh, P. K.; Kumbhakar, M.; Ganguly, R.; Aswal, V. K.; Pal, H.; Nath, S. Time-resolved fluorescence and small angle neutron scattering study in pluronics−surfactant supramolecular assemblies. *J. Phys. Chem. B* **2010**, *114*, 3818−3826.
(23) Hu, C.; Li, R.; Yang, H.; Wang, J. Properties of binary surfactant systems of nonionic surfactants C12E10, C12E23, and C12E42 with a cationic gemini surfactant in aqueous solutions. *J. Colloid Interface Sci.* **2011**, *356*, 605−613.
(24) Vicente, F. A.; Cardoso, I. S.; Sintra, T. E.; Lemus, J.; Marques, E. F.; Ventura, S. P. M.; Coutinho, J. A. P. Impact of surface active ionic liquids on the cloud points of nonionic surfactants and the formation of aqueous micellar two-phase systems. *J. Phys. Chem. B* **2017**, *121*, 8742−8755.
(25) Nambam, J. S.; Philip, J. Effects of interaction of ionic and nonionic surfactants on self-assembly of PEO−PPO−PEO triblock copolymer in aqueous solution. *J. Phys. Chem. B* **2012**, *116*, 1499−1507.
(26) Kihara, S.; van der Heijden, N. J.; Seal, C. K.; Mata, J. P.; Whitten, A. E.; Köper, I.; McGillivray, D. J. Soft and hard interactions between polystyrene nanoplastics and human serum albumin protein corona. *Bioconjugate Chem.* **2019**, *30*, 1067−1076.
(27) Vogel, R.; Pal, A. K.; Jambhrunkar, S.; Patel, P.; Thakur, S. S.; Reategui, E.; Parekh, H. S.; Saa, P.; Stassinopoulos, A.; Broom, M. F. High-resolution single particle zeta potential characterisation of biological nanoparticles using tunable resistive pulse sensing. *Sci. Rep.* **2017**, *7*, 17479.
(28) Griffiths, P. C.; Paul, A.; Khayat, Z.; Heenan, R. K.; Ranganathan, R.; Grillo, I. A small-angle neutron scattering study of biologically relevant mixed surfactant micelles comprising 1, 2-diheptanoyl-sn-phosphatidylcholine and sodium dodecyl sulfate or dodecyltrimethylammonium bromide. *Soft Matter* **2005**, *1*, 152−159.
(29) Pathan, H.; Patil, R.; Ray, D.; Aswal, V. K.; Bahadur, P.; Tiwari, S. Structural changes in non-ionic surfactant micelles induced by ionic liquids and application thereof for improved solubilization of quercetin. *J. Mol. Liq.* **2019**, *290*, 111235.
(30) De, S.; Aswal, V. K.; Goyal, P. S.; Bhattacharya, S. Small-angle neutron scattering studies of different mixed micelles composed of dimeric and monomeric cationic surfactants. *J. Phys. Chem. B* **1997**, *101*, 5639−5645.
(31) Mahajan, R. K.; Vohra, K. K.; Aswal, V. K. Small angle neutron scattering measurements of aggregation behaviour of mixed micelles of conventional surfactants with triblock polymer L64. *Colloids Surf., A* **2008**, *326*, 48−52.
(32) Patil, R.; Marathe, D.; Roy, S. P.; Ray, D.; Aswal, V. K.; Jha, P. K.; Bahadur, P.; Tiwari, S. Colloidal stability of graphene oxide nanosheets in association with triblock copolymers: A neutron scattering analysis. *Mater. Sci. Eng., C* **2020**, *109*, 110559.
(33) Goloub, T. P.; Koopal, L. K. Adsorption of cationic surfactants on silica. Comparison of experiment and theory. *Langmuir* **1997**, *13*, 673−681.
(34) Ray, D.; Kumar, S.; Aswal, V. K.; Kohlbrecher, J. Tuning nanoparticle-micelle interactions and resultant phase behavior. *Langmuir* **2018**, *34*, 259−267.
(35) Yadav, I.; Kumar, S.; Aswal, V.; Kohlbrecher, J. Small-angle neutron scattering study of differences in phase behavior of silica nanoparticles in the presence of lysozyme and bovine serum albumin proteins. *Phys. Rev. E: Stat., Nonlinear, Soft Matter Phys.* **2014**, *89*, 032304.
(36) Kumar, S.; Aswal, V. K.; Kohlbrecher, J. Size-dependent interaction of silica nanoparticles with different surfactants in aqueous solution. *Langmuir* **2012**, *28*, 9288−9297.
(37) Teixeira, J. Small-angle scattering by fractal systems. *J. Appl. Crystallogr.* **1988**, *21*, 781−785.
(38) Yadav, I.; Kumar, S.; Aswal, V. K.; Kohlbrecher, J. Structure and Interaction in the pH-Dependent phase behavior of nanoparticle-protein systems. *Langmuir* **2017**, *33*, 1227−1238.
(39) Yang, B.; Lowe, J. P.; Schweins, R.; Edler, K. J. Small angle neutron scattering studies on the internal structure of poly (lactide-co-glycolide)-block-poly (ethylene glycol) nanoparticles as drug delivery vehicles. *Biomacromolecules* **2015**, *16*, 457−464.
(40) Li, J.; Li, J.; Jiang, L.; Chen, X.; Luo, J. Cationic surfactant micelles lubricate graphitic surface in water. *Langmuir* **2019**, *35*, 11108−11113.
(41) Robinson, B. J.; Bailey, S. W. D.; O'Driscoll, L. J.; Visontai, D.; Welsh, D. J.; Mostert, A. B.; Mazzocco, R.; Rabot, C.; Jarvis, S. P.; Kolosov, O. V.; Bryce, M. R.; Lambert, C. Formation of two-dimensional micelles on graphene: Multi-scale theoretical and experimental study. *ACS Nano* **2017**, *11*, 3404−3412.

https://dx.doi.org/10.1021/acs.langmuir.0c03206
Langmuir 2021, 37, 867−873